




**Infinite-randomness criticality in monitored quantum dynamics with static disorder**Aidan Zabalo <sup>1</sup>, Justin H. Wilson <sup>2</sup>, Michael J. Gullans,<sup>3</sup> Romain Vasseur,<sup>4</sup>  
Sarang Gopalakrishnan,<sup>5</sup> David A. Huse,<sup>6,7</sup> and J. H. Pixley <sup>1,8</sup><sup>1</sup>*Department of Physics and Astronomy, Center for Materials Theory, Rutgers University, Piscataway, New Jersey 08854, USA*<sup>2</sup>*Department of Physics and Astronomy, Center for Computation and Technology,  
Louisiana State University, Baton Rouge, Louisiana 70803, USA*<sup>3</sup>*Joint Center for Quantum Information and Computer Science, NIST/University of Maryland, College Park, Maryland 20742, USA*<sup>4</sup>*Department of Physics, University of Massachusetts, Amherst, Massachusetts 01003, USA*<sup>5</sup>*Department of Physics, The Pennsylvania State University, University Park, Pennsylvania 16802, USA*<sup>6</sup>*Department of Physics, Princeton University, Princeton, New Jersey 08544, USA*<sup>7</sup>*Institute for Advanced Study, Princeton, New Jersey 08540, USA*<sup>8</sup>*Center for Computational Quantum Physics, Flatiron Institute, New York, New York 10010, USA*

(Received 17 June 2022; accepted 7 June 2023; published 23 June 2023)

We consider a model of monitored quantum dynamics with quenched spatial randomness: specifically, random quantum circuits with spatially varying measurement rates. These circuits undergo a measurement-induced phase transition (MIPT) in their entanglement structure, but the nature of the critical point differs drastically from the case with constant measurement rate. In particular, at the critical measurement rate, we find that the entanglement of a subsystem of size  $\ell$  scales as  $S \sim \sqrt{\ell}$ ; moreover, the dynamical critical exponent  $z = \infty$ . The MIPT is flanked by Griffiths phases with continuously varying dynamical exponents. We argue for this infinite-randomness scenario on general grounds and present numerical evidence that it captures some features of the universal critical properties of MIPT using large-scale simulations of Clifford circuits. These findings demonstrate that the relevance and irrelevance of perturbations to the MIPT can naturally be interpreted using a powerful heuristic known as the Harris criterion.

DOI: [10.1103/PhysRevB.107.L220204](https://doi.org/10.1103/PhysRevB.107.L220204)

*Introduction.* Recent years have seen dramatic advances in the assembly and control of quantum coherent matter [1–3], demonstrating significant progress towards a universal quantum computer and other practical quantum technologies. These systems lead to new paradigms for many-body physics in which phases of matter can be defined in a purely information-theoretic manner [4–6], raising fundamental questions about the role of the environment or “observer” in quantum many-body physics. Theoretical efforts in this area have focused on the behavior of monitored systems where there is a threshold for fault tolerance characterized by a dynamic phase transition in the entanglement [7–9]. However, as exhibited by recent experiments [10–12], any physical realization will have spatially random noise in some aspect of the device (e.g., due to fabrication or read-out imperfections). Such noise appears as static disorder at the level of a monitored quantum circuit, which could have a significant effect on the fault-tolerance thresholds and associated phases.

As a toy model for monitored quantum systems and their associated criticality, the study of “hybrid” dynamics (i.e., unitary evolution interspersed with measurements) in random quantum circuits has garnered a significant amount of attention in recent years [6,13–15]. It has become well established that the competition between scrambling (unitary) dynamics and local measurements leads to a measurement-induced phase transition (MIPT)—a phase transition in the entanglement structure of the quantum state conditional on a set of (typical) measurement outcomes. Previous studies

established properties of MIPTs with a uniform density of measurements [13,14,16–53], but do not address physical situations where some qubits are preferentially measured over others (e.g., qubits closer to transmission lines, or computation with a measuring adversary who has limited access to some of the qubits). In this Letter, we find that when qubits are preferentially measured with individual probabilities  $p_x$ , the phases and transition change dramatically, flowing to an infinite-randomness fixed point.

In special limits, such as the Hartley entropy for generic (Haar) random circuits [14] or infinite on-site Hilbert space dimension [17], the physics of the MIPT in  $d$  dimensions can be understood via mappings to percolation in  $d + 1$  dimensions. In the case of a  $d = 1$  spin chain, the quenched spatial randomness (i.e., preferential measurements) corresponds to columnar disorder in the two-dimensional lattice. Applying the rigorous Chayes-Chayes-Fisher-Spencer (CCFS) bound [54] for disordered systems indicates that the correlation length exponent  $\nu$ , which characterizes the divergence of the characteristic length scale as the critical point is approached, should satisfy  $\nu \geq 2/d$  for the critical point to remain stable upon the introduction of disorder. Taking  $\nu = 4/3$  for percolation, shows that the critical point is unstable and has been found to flow to infinite randomness [55]. This behavior is not seen for uncorrelated disorder since the dimension is instead  $d + 1$ , and therefore the CCFS bound is satisfied. Away from the percolation limits, numerical studies of MIPTs yield  $\nu \approx 1.3$  [13,16,19,20,23], and therefore we expect a violation of

the CCFS bound with quenched spatial randomness. Indeed, we demonstrate that the MIPT flows to a critical, infinite-disorder, universality class and uncover the nearby Griffiths phases that control the dynamics of quantum information. Moreover, we establish the irrelevance of static quasiperiodicity, consistent with the Luck criteria [56] ( $\nu \geq 1/d$ ) (see Sec. S1 in the Supplemental Material [57]).

We pursue two complementary approaches: First, we explore classically simulable Clifford circuits with a spatially varying measurement rate; second, we construct a real-space renormalization-group (RSRG) treatment [58–62] that is strictly valid in the limit of large on-site Hilbert space dimensions, but that may describe the fixed point more generally. The two approaches are mutually consistent in many respects, but qualitative deviations between the two critical points are found in some observables.

The RSRG mapping yields the following universal predictions: (i) This critical point exhibits activated dynamical scaling, i.e., space and timescale with the relation  $\ln t \sim \sqrt{x}$  [cf. the relativistic behavior at the conventional MIPT ( $x \sim t$ )]; (ii) the steady-state entanglement of a subsystem of size  $\ell$  at the critical point scales as  $S(\ell) \sim \sqrt{\ell}$  [cf.  $\sim \ln \ell$  in the absence of static disorder]; (iii) the MIPT is flanked by Griffiths phases in which the late-time dynamics is governed by rare-region effects. We put forward these three behaviors as sufficient criteria to claim two critical points are described by the same infinite-randomness fixed point. Our numerical evidence indicates that both Clifford circuits and percolation are consistent with each of these predictions. However, we also find that the tripartite information at the Clifford critical point acquires a broad distribution, with its average growing as a fractional power law of system size. This numerical observation appears robust, and goes beyond any existing theoretical calculation. This feature also appears to be absent in our numerical simulations of percolation with columnar disorder.

*Models and entanglement probes of the MIPT.* We consider random circuit models with the “brick wall” structure consisting of randomly chosen two-qubit gates between nearest-neighbor  $q$ -state spins. For our numerical simulations, our two-qubit gates are Clifford gates ( $q = 2$ ), allowing us to reach large system sizes with efficient classical simulations [63–66] (all simulations have periodic boundary conditions). Our analytic treatment uses Haar-random gates, and we send  $q \rightarrow \infty$ . Last, we also consider a classical limit of this model by solving a percolation problem with columnar disorder (see Sec. S3 [57]).

To build static spatial randomness into the problem we use a position-dependent measurement probability  $p_x$  applied between every layer of unitary gates and given by  $p_x = \mathbf{r}_x^n$ , where  $\mathbf{r}_x$  is a random variable uniformly distributed in  $[0, 1]$  and  $n$  is the tuning parameter. We denote averages over circuit realizations via  $\overline{\dots}$ . For a given realization of the circuit, we generate the static  $p_x$  and parametrize the strength of the measurement rate by its disorder-averaged value, i.e.,  $\bar{p} = \frac{1}{n+1}$ . This distribution is chosen to have long tails so that rare regions of atypical values of  $p_x$  play an important role in the dynamics for modest system sizes, but we do not expect it to change the universal properties of the critical point in the thermodynamic limit. This static measurement profile produces a “columnar” disorder pattern in space-time.

The measurement transition is present in averaged quantities that are nonlinear in the reduced density matrix conditional on measurement outcomes, therefore we focus on entanglement probes of the system. First, the von Neumann entanglement entropy  $S(x, t)$  is computed by dividing our system into two regions  $A$  (of length  $x$ ) and  $B$  (of length  $L - x$ ), resulting in  $S(x, t) = -\text{Tr}_A[\rho_A \log_2 \rho_A]$ , where  $\rho_A = \text{Tr}_B|\psi(t)\rangle\langle\psi(t)|$  is a trace of the density matrix over region  $B$  and  $|\psi(t)\rangle$  is the time-evolved wave function on a given sampled quantum trajectory. Unless otherwise specified, we choose the initial state of the system to be a random product state of up- and down-spin sites. In stabilizer circuits, von Neumann and Rényi entropies are identical, but we expect similar results for any Rényi entropy  $S_n$  in other cases (e.g., Haar) since their values must scale similarly with system size [differing by at most a constant  $n/(n-1)$ ] [14].

Second, to identify and characterize the critical point of the entanglement transition, we use the tripartite mutual information  $\bar{\mathcal{I}}_3(A, B, C) \equiv S(A) + S(B) + S(C) - S(A \cup B) - S(A \cup C) - S(B \cup C) + S(A \cup B \cup C)$  where we have omitted the time label and have partitioned the system into adjacent regions  $A, B, C$  each of size  $L/4$ . The value of  $\bar{\mathcal{I}}_3$  depends sensitively on the circuit realization; we thus study a probability distribution  $P[\bar{\mathcal{I}}_3]$  over trajectories and circuit realizations, in addition to the circuit-averaged value  $\bar{\bar{\mathcal{I}}}_3$ . With strong spatial randomness the mean  $\bar{\bar{\mathcal{I}}}_3$  is not representative of the broad distribution  $P[\bar{\mathcal{I}}_3]$  due to fat tails. Thus, studying the distribution  $P[\bar{\mathcal{I}}_3]$  in detail, we are motivated to generalize the scaling ansatz from Refs. [16,19] to include the possibility of extensive scaling at the critical point (see supporting distribution data in Sec. S2A [57]). Consequently, to numerically identify the critical point, we find it most accurate to analyze the distribution  $P[\bar{\mathcal{I}}_3]$ .

We study the purification dynamics of the ancilla order parameter defined by Ref. [67]: At  $t = 0$  a site in the system is maximally entangled with a reference qubit and the system is scrambled by unitary evolution for a time  $2L$ . The system is then evolved under the hybrid dynamics for an additional time  $2L$  and the average entanglement entropy of the reference qubit  $\bar{S}_Q$  acts as an order parameter. Near the critical point,  $\bar{S}_Q$  obeys single-parameter scaling allowing for an additional probe of the transition complementary to  $\bar{\mathcal{I}}_3$ .

*RSRG for quenched disorder.* The transition is analytically tractable for Haar-random circuits as the on-site Hilbert space  $q \rightarrow \infty$ , using mappings onto replica statistical mechanics models [17,35,40,68–70]. Upon averaging over random Haar gates and measurement locations and outcomes, nonlinear functions of the density matrix can be mapped onto an effective two-dimensional  $k!$ -state Potts model in the replica limit  $k \rightarrow 1$ , which describes *bond percolation* [17,35]. Quenched disorder in the circuit leads to *columnar disorder* in the statistical mechanics model, which is amenable to RSRG techniques [57,58,60]. We find that for any number of replicas, and directly in the replica limit  $k \rightarrow 1$ , the transition is described by an infinite-randomness fixed point [57] with space-time scaling  $\ln t \sim \ell^\psi$ , with  $\psi = \frac{1}{2}$  ( $z = \infty$  that diverges as  $z \sim \ell^\psi / \ln \ell$ ), in agreement with results on percolation with columnar disorder [55]. Scaling properties follow from known results [58–60]: In particular, the (average) correlation length exponent is

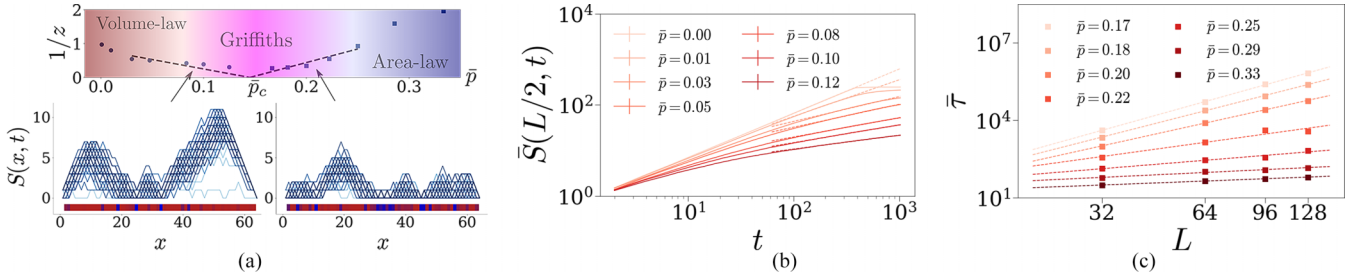


FIG. 1. (a) Top: Phase diagram of the disordered circuit model indicating the behavior of the dynamic exponent  $z$ , which characterizes the divergence of the characteristic timescale, near the critical point and Griffiths phase. The dynamic exponent  $z = z(\bar{p})$  is a continuous function of the average measurement rate  $\bar{p}$  and increases as  $\bar{p} \rightarrow \bar{p}_c$  from the volume-law and area-law phases (data points are obtained from numerical simulations, dashed lines are the result of the RSRG prediction  $1/z \sim |p - p_c|^{\nu\psi} = |p - p_c|$ ). Bottom: Entanglement profile  $S(x, t)$  as a function of the cut  $x$  and time  $t$  (darker blue indicates later times). Each panel corresponds to a single trajectory and a different value of  $\bar{p}$  in the Griffiths regime (left:  $\bar{p} = 0.091$ ; right:  $\bar{p} = 0.20$ ). The red to blue color at the bottom indicates small to large values of the local measurement probability  $p_x$ , respectively. (b) Early-time behavior of the average half-cut entanglement entropy,  $\bar{S}(L/2, t)$ , in the volume-law phase of the disordered circuit. The data are fit to a power law given by  $\bar{S}(L/2, t) \sim t^{1/z}$ . (c) Purification time in the area-law phase used to extract the dynamical exponent from a fit of  $\bar{\tau} \sim L^z$ .

$\nu = 2$ , and the scaling in the phases is controlled by Griffiths effects.

Importantly, the mapping predicts that the steady-state entanglement entropy at criticality scales as  $\bar{S} \sim \sqrt{\ell}$ . In the statistical mechanics picture, the entanglement entropy is related to the free-energy cost of inserting a domain wall of size  $\ell$  at the (spatial) boundary of the system [17,35]; this cost is related to the *logarithm* of the boundary two-point function, which typically scales as  $\exp(-\ell^\psi)$  [58–60]. Since  $\bar{S}$  is related to the logarithm of the boundary two-point function it is dominated by typical samples and not rare samples, hence the result above. Furthermore, due to space-time scaling  $\ln t \sim \sqrt{\ell}$ ,  $\bar{S} \sim \ln t$ .

Although our predictions are restricted to  $q = \infty$ , infinite-randomness fixed points are typically “superuniversal” [71,72], e.g., in the random Potts model the critical properties independent of the number of states [71], in contrast with the clean case. We therefore expect our  $q = \infty$  predictions to extend to finite  $q$ , which we verify numerically below for qubits ( $q = 2$ ). Notably, however, we find deviations between the universal behavior of the  $q = \infty$  percolation model and the Clifford model in the scaling of mutual information quantities at criticality.

**Griffiths phases.** The RSRG treatment predicts that around the critical point, certain dynamical quantities are dominated by rare-region effects. The presence of rare-region effects is manifest in spatial profiles of the entanglement entropy  $S(x, t)$  for a given profile of measurement rates (for position  $x$  and time  $t$ ) [see Fig. 1(a)]. At small values of  $\bar{p}$ , frequently measured regions act as bottlenecks that hinder the growth of the entanglement. In contrast, for large values of  $\bar{p}$  we see that regions that are measured infrequently produce highly scrambled local regions. (Note that Griffiths effects in measurement-induced phases were previously studied, in “flipped” circuits with the roles of space and time interchanged [73]. Relating the two sets of results is an interesting task for future work.)

The observables that diagnose these Griffiths effects are distinct in the two phases. In the volume-law phase, regions with a high measurement probability act as bottlenecks for

*entanglement growth*. Conversely, in the area-law phase, rare locally scrambling regions dominate *the purification rate* of an initially mixed state.

First, consider the volume-law phase and a region of size  $\ell$  that is locally in the area-law phase and gets entangled with degrees of freedom to its left; therefore, it is in a mixed state. Measurements rapidly purify/disentangle this region, and the probability (and therefore the rate) that entanglement spreads across it scales as  $e^{-\ell/\xi}$  where  $\xi$  is the local correlation length inside the rare region. Because the measurement rate is spatially uncorrelated, the density of rare regions of size  $\ell$  is exponentially suppressed as  $f^\ell$  for some  $f$  that depends on the microscopic details of the disorder but approaches unity at the transition. Therefore, bottlenecks that allow entanglement growth at rate  $\leq \gamma$  occur at density  $f^{-\xi \ln \gamma} \sim \gamma^\alpha$ , where  $\alpha \equiv \xi |\ln f|$ . Reference [74] addressed the problem of entanglement growth in the presence of a power-law distribution of bottlenecks and found that  $\bar{S}(t) \sim t^{1/z}$ , where  $z = (\alpha + 1)/\alpha$ . In Fig. 1(b), the late-time entanglement growth is shown along with a power-law fit at late times to extract  $z$  in the volume-law phase. This stands in stark contrast to space-time random circuits that scale ballistically in time.

Next, consider the area-law phase and a region of size  $\ell$  that is locally in the volume-law phase; it purifies on a timescale  $\sim e^{\ell/\xi}$  where  $\xi$  is the local correlation length of the region. As before, the density of volume-law regions of size  $\ell$  is suppressed as  $\tilde{f}^\ell$  for some  $\tilde{f}$  that approaches unity at the transition. In a sample of size  $L$ , the largest expected volume-law region has  $\tilde{f}^\ell \sim 1/L$  so  $\ell \sim \ln L / |\ln \tilde{f}|$ . The purification time of the sample is controlled by this largest bottleneck and therefore scales as  $\tau(L) \sim L^z$  where  $z = 1/(\xi |\ln \tilde{f}|)$ . Deep in the area-law phase  $z \rightarrow 0$  but as  $\bar{p} \rightarrow \bar{p}_c$  rare-region effects begin to play a role in the dynamics and the size of the largest rare region determines the purification time, giving rise to the power-law behavior  $\bar{\tau} \sim L^z$ . In Fig. 1(c),  $z$  is extracted via fits to the largest system sizes.

In summary, in each Griffiths regime the dynamic exponent  $z = z(\bar{p})$  is a continuously varying function of  $\bar{p}$ ; it diverges as  $p \rightarrow p_c$  from both sides, starting from  $z = 1$  ( $z = 0$ ) in the deep volume- (area-) law phase [see Fig. 1(a)]. These results

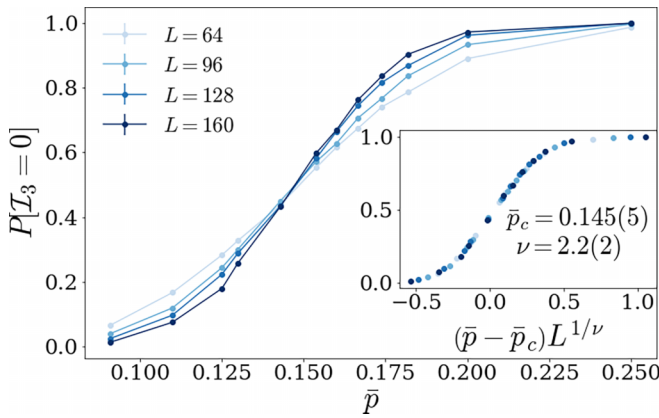


FIG. 2. Data and collapse of the distribution  $P[\mathcal{I}_3 = 0]$  used to determine the critical point  $\bar{p}_c$  and the correlation length exponent  $\nu$ .

provide an underestimate of  $z$  near  $\bar{p}_c$  as it is heavily affected by finite-size effects.

*Identifying the critical point and its properties.* Next, we determine the location of the critical point using the tripartite mutual information. Due to the distribution  $P[\mathcal{I}_3]$  developing fat tails (see Sec. S2A [57]), the mean  $\bar{\mathcal{I}}_3$  does not fully characterize the distribution, which dramatically modifies the single-parameter scaling  $\bar{\mathcal{I}}_3$  near the transition. Therefore, we turn to properties of  $P[\mathcal{I}_3]$  to identify  $\bar{p}_c$ . In the volume-law phase, the probability to find  $\mathcal{I}_3 = 0$  must vanish in the thermodynamic limit, whereas it must approach unity deep in the area-law phase (see Sec. S2A [57]). As shown in Fig. 2, this behavior is consistent with our numerical data allowing us to identify  $P[\mathcal{I}_3 = 0]$  as a scaling variable, which importantly does not require knowing the scaling of  $\bar{\mathcal{I}}_3$ . Using the scaling ansatz  $P[\mathcal{I}_3 = 0] \sim F[L^{1/\nu}(\bar{p} - \bar{p}_c)]$ , where  $F(x)$  is an arbitrary scaling function, we find excellent data collapse as shown in Fig. 2 (inset) for  $\bar{p}_c \approx 0.145(5)$  and  $\nu \approx 2.2(2)$ , in agreement with the RSRG. Importantly, the estimated value of  $\nu$  is stable with respect to the Harris/CCFS bound.

Furthermore, we can use the data collapse of  $\bar{\mathcal{I}}_3$  with the less constrained scaling ansatz  $\bar{\mathcal{I}}_3 \sim L^\alpha g[(\bar{p} - \bar{p}_c)L^{1/\nu}]$ , to account for  $L$  dependence at the critical point, that could be incurred for example due to a fat tail in  $P[\mathcal{I}_3]$ . For completeness, we consider three cases of the scaling function motivated by

generality, the behavior of  $P[\mathcal{I}_3 = 0]$ , and the RSRG picture (see Sec. S2B [57]). In all cases, we find similar results for  $\bar{p}_c$ ,  $\nu$ , and  $\alpha > 0$  with differences  $\lesssim 10\%$ . Last, the nonzero value of  $\alpha$  is beyond the classical limit of the model (see Sec. S3B [57]).

Motivated by these results, we study the average, half-cut, bipartite entanglement entropy  $\bar{S}(L/2, t)$  as a function of the system size  $L$  and time  $t$ . Near the transition ( $\bar{p} \approx \bar{p}_c$ ) we find

$$\bar{S}(L/2, t \gg L) \sim \sqrt{L} \quad \text{and} \quad \bar{S}(L/2 \gg t, t) \sim \ln t, \quad (1)$$

as shown in Fig. 3(a), in agreement with the RSRG predictions. These results demonstrate that the critical point has a divergent dynamic exponent consistent with an infinite-randomness fixed point. In the classical limit of percolation, we have also found the scaling in Eqs. (1) (see Sec. S3B [57]). Additionally, we compute the saturation time  $t_*$  at which  $\bar{S}(L/2, t)$  reaches its late-time value as shown in Fig. 3(b). In the disordered system, rare regions cause the entanglement to grow sub-ballistically so that the saturation time is no longer  $t_* \sim L$ . Numerically, in the volume-law phase, we find a stretched exponential  $t_* \sim e^{\sqrt{L}}$  while in the area-law phase it approaches a constant [see Fig. 3(b) (inset)].

Finally, the average order parameter dynamics  $\bar{S}_Q(t, L)$  at the critical point is shown in Fig. 3(c). Our results demonstrate this critical point is of the infinite-randomness type and has a divergent dynamic exponent  $z \sim \xi^\psi \sim |\bar{p} - \bar{p}_c|^{-\nu\psi}$ ; therefore, we can use the activated dynamic scaling ansatz [75] that yields  $\bar{S}_Q(t, L) \sim g(L^{-\psi} \ln t)$ , where  $g(x)$  is an arbitrary scaling function and  $\psi$  is the so-called activation or barrier exponent. We find  $\psi = 0.56(4)$  through data collapse [see Fig. 3(c) (inset)]. Importantly, this value of  $\psi$  is in agreement with RSRG and consistent with the length-time scaling of the entanglement entropy in Eq. (1).

*Discussion.* Introducing static disorder to the measurement-induced phase transition is a relevant perturbation that produces a flow to an (apparently) infinite-randomness critical point. We developed a real-space renormalization group approach to this transition and verified its predictions using large-scale simulations of Clifford circuits and its classical limit through percolation. Our results for the tripartite mutual information for Clifford circuits and percolation show qualitatively different behavior, suggesting that these two infinite-randomness fixed points belong

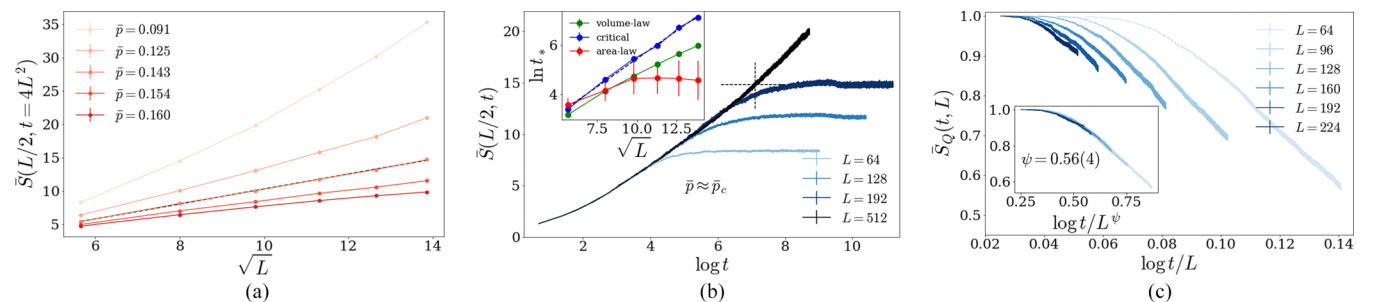


FIG. 3. (a) Average half-cut entanglement entropy at late times for various measurement rates. Near the critical point, the entanglement entropy behaves as  $\bar{S} \sim \sqrt{L}$  as shown by the black dotted line fit for  $\bar{p}_c \approx 0.14$ . (b) Example fit (at  $\bar{p} \approx \bar{p}_c$ ) used to extract the saturation time  $t_*$  as a function of system size. Inset: In the volume-law phase, we find a stretched exponential behavior  $t_* \sim \exp[\sqrt{L}]$  while in the area-law phase it approaches a constant. (c) Order parameter dynamics for the disordered measurement rate. The data collapse onto a single universal curve using the activated dynamic scaling ansatz.

to distinct universality classes. Analytically, computing this quantity within the RSRG is an important task for future work.

Our results for static randomness stand in stark contrast with the case of static quasiperiodic modulation in space. The relevance of quasiperiodic perturbations added to random circuits is governed by the weaker Luck [56] bound  $\nu \geq 1/d$ . Therefore, quasiperiodic spatial modulations of the measurement rate leave the universal nature of the MIPT unchanged, as we demonstrate in Sec. S1 [57]. The demonstration of the Harris/Luck criteria to measurement-induced criticality provides a powerful heuristic to interpret relevant and irrelevant perturbations on this information-theoretic transition. Under this paradigm, future work could begin to understand how topologically ordered phases and transitions change with static randomness [20].

Finally, we remark that many quantum computing systems exhibit quenched spatial randomness in the noise and tuning parameters due to disorder in device fabrication [11]; therefore, we expect some of the universal features studied here

to be relevant in the many-body physics of such devices. We leave more concrete studies of these effects for future work.

*Acknowledgments.* A.Z. was supported by a HEERF graduate fellowship, and J.H.P. and R.V. were supported by the Alfred P. Sloan Foundation through Sloan Research Fellowships. We acknowledge support from NSF Grants No. DMR-2103938 (S.G.) and No. DMR-2104141 (R.V.), and QLCI Grant No. OMA-2120757 (M.J.G., D.A.H.). R.V. thanks A. C. Potter and S. A. Parameswaran for discussions of RSRG. The authors acknowledge the Beowulf cluster at the Department of Physics and Astronomy of Rutgers University and the Office of Advanced Research Computing (OARC) at Rutgers, The State University of New Jersey [76] for providing access to the Amarel cluster, and associated research computing resources that have contributed to the results reported here. Part of this research was done using services provided by the OSG Consortium [77,78], which is supported by the National Science Foundation Awards No. 2030508 and No. 1836650.

- 
- [1] Y. Alexeev, D. Bacon, K. R. Brown, R. Calderbank, L. D. Carr, F. T. Chong, B. DeMarco, D. Englund, E. Farhi, B. Fefferman, A. V. Gorshkov, A. Houck, J. Kim, S. Kimmel, M. Lange, S. Lloyd, M. D. Lukin, D. Maslov, P. Maunz, C. Monroe *et al.*, Quantum computer systems for scientific discovery, *PRX Quantum* **2**, 017001 (2021).
- [2] E. Altman, K. R. Brown, G. Carleo, L. D. Carr, E. Demler, C. Chin, B. DeMarco, S. E. Economou, M. A. Eriksson, K.-M. C. Fu, M. Greiner, K. R. A. Hazzard, R. G. Hulet, A. J. Kollár, B. L. Lev, M. D. Lukin, R. Ma, X. Mi, S. Misra, C. Monroe *et al.*, Quantum simulators: Architectures and opportunities, *PRX Quantum* **2**, 017003 (2021).
- [3] D. Awschalom, K. K. Berggren, H. Bernien, S. Bhave, L. D. Carr, P. Davids, S. E. Economou, D. Englund, A. Faraon, M. Fejer, S. Guha, M. V. Gustafsson, E. Hu, L. Jiang, J. Kim, B. Korzh, P. Kumar, P. G. Kwiat, M. Lončar, M. D. Lukin *et al.*, Development of quantum interconnects (QuICs) for next-generation information technologies, *PRX Quantum* **2**, 017002 (2021).
- [4] D. Aharonov, Quantum to classical phase transition in noisy quantum computers, *Phys. Rev. A* **62**, 062311 (2000).
- [5] M. P. A. Fisher, V. Khemani, A. Nahum, and S. Vijay, Random quantum circuits, *Annu. Rev. Condens. Matter Phys.* **14**, 335 (2023).
- [6] A. C. Potter and R. Vasseur, Entanglement dynamics in hybrid quantum circuits, in *Entanglement in Spin Chains*, Quantum Science and Technology (Springer, Cham, 2022), pp. 211–249.
- [7] D. Aharonov and M. Ben-Or, Fault-tolerant quantum computation with constant error, in *Proceedings of the Twenty-Ninth Annual ACM Symposium on Theory of Computing - STOC '97* (ACM Press, New York, 1997), pp. 176–188.
- [8] E. Dennis, A. Kitaev, A. Landahl, and J. Preskill, Topological quantum memory, *J. Math. Phys.* **43**, 4452 (2002).
- [9] D. Gottesman, An introduction to quantum error correction and fault-tolerant quantum computation, in *Quantum Information Science and Its Contributions to Mathematics*, Proceedings of Symposia in Applied Mathematics (Amer. Math. Soc., Providence, Rhode Island, 2010), Vol. 68, pp. 13–58.
- [10] L. Egan, D. M. Debroy, C. Noel, A. Risinger, D. Zhu, D. Biswas, M. Newman, M. Li, K. R. Brown, M. Cetina, and C. Monroe, Fault-tolerant control of an error-corrected qubit, *Nature (London)* **598**, 281 (2021).
- [11] S. Krinner, N. Lacroix, A. Remm, A. D. Paolo, E. Genois, C. Leroux, C. Hellings, S. Lazar, F. Swiadek, J. Herrmann, G. J. Norris, C. K. Andersen, M. Müller, A. Blais, C. Eichler, and A. Wallraff, Realizing repeated quantum error correction in a distance-three surface code, *Nature (London)* **605**, 669 (2022).
- [12] R. Acharya, I. Aleiner, R. Allen, T. I. Andersen, M. Ansmann, F. Arute, K. Arya, A. Asfaw, J. Atalaya, R. Babbush, D. Bacon, J. C. Bardin, J. Basso, A. Bengtsson, S. Boixo, G. Bortoli, A. Bourassa, J. Bovaird, L. Brill, M. Broughton *et al.*, Suppressing quantum errors by scaling a surface code logical qubit, *Nature* **614**, 676 (2023).
- [13] Y. Li, X. Chen, and M. P. A. Fisher, Measurement-driven entanglement transition in hybrid quantum circuits, *Phys. Rev. B* **100**, 134306 (2019).
- [14] B. Skinner, J. Ruhman, and A. Nahum, Measurement-Induced Phase Transitions in the Dynamics of Entanglement, *Phys. Rev. X* **9**, 031009 (2019).
- [15] C. Noel, P. Niroula, D. Zhu, A. Risinger, L. Egan, D. Biswas, M. Cetina, A. V. Gorshkov, M. J. Gullans, D. A. Huse, and C. Monroe, Measurement-induced quantum phases realized in a trapped-ion quantum computer, *Nat. Phys.* **18**, 760 (2022).
- [16] M. J. Gullans and D. A. Huse, Dynamical Purification Phase Transition Induced by Quantum Measurements, *Phys. Rev. X* **10**, 041020 (2020).
- [17] C.-M. Jian, Y.-Z. You, R. Vasseur, and A. W. W. Ludwig, Measurement-induced criticality in random quantum circuits, *Phys. Rev. B* **101**, 104302 (2020).
- [18] Y. Li, X. Chen, A. W. W. Ludwig, and M. P. A. Fisher, Conformal invariance and quantum nonlocality in critical hybrid circuits, *Phys. Rev. B* **104**, 104305 (2021).
- [19] A. Zabalo, M. J. Gullans, J. H. Wilson, S. Gopalakrishnan, D. A. Huse, and J. H. Pixley, Critical properties of the measurement-induced transition in random quantum circuits, *Phys. Rev. B* **101**, 060301(R) (2020).

- [20] A. Lavasani, Y. Alavirad, and M. Barkeshli, Measurement-induced topological entanglement transitions in symmetric random quantum circuits, *Nat. Phys.* **17**, 342 (2021).
- [21] Y. Bao, S. Choi, and E. Altman, Symmetry enriched phases of quantum circuits, *Ann. Phys.* **435**, 168618 (2021).
- [22] Y. Li and M. P. A. Fisher, Robust decoding in monitored dynamics of open quantum systems with  $Z_2$  symmetry, [arXiv:2108.04274](https://arxiv.org/abs/2108.04274).
- [23] U. Agrawal, A. Zabalo, K. Chen, J. H. Wilson, A. C. Potter, J. H. Pixley, S. Gopalakrishnan, and R. Vasseur, Entanglement and Charge-Sharpener Transitions in  $U(1)$  Symmetric Monitored Quantum Circuits, *Phys. Rev. X* **12**, 041002 (2022).
- [24] F. Barratt, U. Agrawal, S. Gopalakrishnan, D. A. Huse, R. Vasseur, and A. C. Potter, Field Theory of Charge Sharpening in Symmetric Monitored Quantum Circuits, *Phys. Rev. Lett.* **129**, 120604 (2022).
- [25] M. Ippoliti, M. J. Gullans, S. Gopalakrishnan, D. A. Huse, and V. Khemani, Entanglement Phase Transitions in Measurement-Only Dynamics, *Phys. Rev. X* **11**, 011030 (2021).
- [26] A. Lavasani, Y. Alavirad, and M. Barkeshli, Topological order and Criticality in  $(2+1)$ D Monitored Random Quantum Circuits, *Phys. Rev. Lett.* **127**, 235701 (2021).
- [27] M. Van Regemortel, Z.-P. Cian, A. Seif, H. Dehghani, and M. Hafezi, Entanglement Entropy Scaling Transition under Competing Monitoring Protocols, *Phys. Rev. Lett.* **126**, 123604 (2021).
- [28] N. Lang and H. P. Büchler, Entanglement transition in the projective transverse field Ising model, *Phys. Rev. B* **102**, 094204 (2020).
- [29] S. Sang and T. H. Hsieh, Measurement-protected quantum phases, *Phys. Rev. Res.* **3**, 023200 (2021).
- [30] S. Choi, Y. Bao, X.-L. Qi, and E. Altman, Quantum Error Correction in Scrambling Dynamics and Measurement-Induced Phase Transition, *Phys. Rev. Lett.* **125**, 030505 (2020).
- [31] O. Lunt, M. Szyniszewski, and A. Pal, Measurement-induced criticality and entanglement clusters: A study of one-dimensional and two-dimensional Clifford circuits, *Phys. Rev. B* **104**, 155111 (2021).
- [32] O. Alberton, M. Buchhold, and S. Diehl, Entanglement Transition in a Monitored Free-Fermion Chain: From Extended Criticality to Area Law, *Phys. Rev. Lett.* **126**, 170602 (2021).
- [33] M. Szyniszewski, A. Romito, and H. Schomerus, Entanglement transition from variable-strength weak measurements, *Phys. Rev. B* **100**, 064204 (2019).
- [34] Y. Li, X. Chen, and M. P. A. Fisher, Quantum Zeno effect and the many-body entanglement transition, *Phys. Rev. B* **98**, 205136 (2018).
- [35] Y. Bao, S. Choi, and E. Altman, Theory of the phase transition in random unitary circuits with measurements, *Phys. Rev. B* **101**, 104301 (2020).
- [36] O. Lunt and A. Pal, Measurement-induced entanglement transitions in many-body localized systems, *Phys. Rev. Res.* **2**, 043072 (2020).
- [37] S. Goto and I. Danshita, Measurement-induced transitions of the entanglement scaling law in ultracold gases with controllable dissipation, *Phys. Rev. A* **102**, 033316 (2020).
- [38] Q. Tang and W. Zhu, Measurement-induced phase transition: A case study in the nonintegrable model by density-matrix renormalization group calculations, *Phys. Rev. Res.* **2**, 013022 (2020).
- [39] X. Cao, A. Tilloy, and A. D. Luca, Entanglement in a fermion chain under continuous monitoring, *SciPost Phys.* **7**, 24 (2019).
- [40] A. Nahum, S. Roy, B. Skinner, and J. Ruhman, Measurement and entanglement phase transitions in all-to-all quantum circuits, on quantum trees, and in Landau-Ginsburg theory, *PRX Quantum* **2**, 010352 (2021).
- [41] X. Turkeshi, R. Fazio, and M. Dalmonte, Measurement-induced criticality in  $(2+1)$ -dimensional hybrid quantum circuits, *Phys. Rev. B* **102**, 014315 (2020).
- [42] L. Zhang, J. A. Reyes, S. Kourtis, C. Chamon, E. R. Mucciolo, and A. E. Ruckenstein, Nonuniversal entanglement level statistics in projection-driven quantum circuits, *Phys. Rev. B* **101**, 235104 (2020).
- [43] M. Szyniszewski, A. Romito, and H. Schomerus, Universality of Entanglement Transitions from Stroboscopic to Continuous Measurements, *Phys. Rev. Lett.* **125**, 210602 (2020).
- [44] Y. Fuji and Y. Ashida, Measurement-induced quantum criticality under continuous monitoring, *Phys. Rev. B* **102**, 054302 (2020).
- [45] D. Rossini and E. Vicari, Measurement-induced dynamics of many-body systems at quantum criticality, *Phys. Rev. B* **102**, 035119 (2020).
- [46] S. Vijay, Measurement-driven phase transition within a volume-law entangled phase, [arXiv:2005.03052](https://arxiv.org/abs/2005.03052).
- [47] X. Turkeshi, A. Biella, R. Fazio, M. Dalmonte, and M. Schiró, Measurement-induced entanglement transitions in the quantum Ising chain: From infinite to zero clicks, *Phys. Rev. B* **103**, 224210 (2021).
- [48] A. Zabalo, M. J. Gullans, J. H. Wilson, R. Vasseur, A. W. W. Ludwig, S. Gopalakrishnan, D. A. Huse, and J. H. Pixley, Operator Scaling Dimensions and Multifractality at Measurement-Induced Transitions, *Phys. Rev. Lett.* **128**, 050602 (2022).
- [49] P. Sierant, G. Chiriaco, F. M. Surace, S. Sharma, X. Turkeshi, M. Dalmonte, R. Fazio, and G. Pagano, Dissipative Floquet dynamics: From steady state to measurement induced criticality in trapped-ion chains, *Quantum* **6**, 638 (2022).
- [50] S. Sharma, X. Turkeshi, R. Fazio, and M. Dalmonte, Measurement-induced criticality in extended and long-range unitary circuits, *SciPost Phys. Core* **5**, 023 (2022).
- [51] X. Chen, Non-unitary free boson dynamics and the boson sampling problem, [arXiv:2110.12230](https://arxiv.org/abs/2110.12230).
- [52] Y. Han and X. Chen, Measurement-induced criticality in  $Z_2$ -symmetric quantum automaton circuits, *Phys. Rev. B* **105**, 064306 (2022).
- [53] J. Iaconis, A. Lucas, and X. Chen, Measurement-induced phase transitions in quantum automaton circuits, *Phys. Rev. B* **102**, 224311 (2020).
- [54] J. T. Chayes, L. Chayes, D. S. Fisher, and T. Spencer, Finite-Size Scaling and Correlation Lengths for Disordered Systems, *Phys. Rev. Lett.* **57**, 2999 (1986).
- [55] R. Juhász and F. Igloi, Percolation in a random environment, *Phys. Rev. E* **66**, 056113 (2002).
- [56] J. Luck, A classification of critical phenomena on quasicrystals and other aperiodic structures, *Europhys. Lett.* **24**, 359 (1993).
- [57] See Supplemental Material at <http://link.aps.org/supplemental/10.1103/PhysRevB.107.L220204> for results for the critical properties of the quasiperiodic model, distribution of  $T_3$  and alternative identification of the critical point for the disordered circuit model, results for the critical properties of the

- percolation model and details of the numerical algorithm, and details about the statistical mechanics model and RSRG.
- [58] D. S. Fisher, Random Transverse Field Ising Spin Chains, *Phys. Rev. Lett.* **69**, 534 (1992).
- [59] D. S. Fisher, Critical behavior of random transverse-field Ising spin chains, *Phys. Rev. B* **51**, 6411 (1995).
- [60] D. S. Fisher, Random antiferromagnetic quantum spin chains, *Phys. Rev. B* **50**, 3799 (1994).
- [61] F Iglói and C. Monthus, Strong disorder RG approach of random systems, *Phys. Rep.* **412**, 277 (2005).
- [62] G. Refael and E. Altman, Strong disorder renormalization group primer and the superfluid–insulator transition, *C. R. Phys.* **14**, 725 (2013).
- [63] D. Gottesman, The Heisenberg representation of quantum computers, in *Group 22: Proceedings of the XXII International Colloquium on Group Theoretical Methods in Physics*, edited by S. P. Corney, R. Delbourgo, and P. D. Jarvis (International Press of Boston, Somerville, MA, 1999), pp. 32–43.
- [64] S. Aaronson and D. Gottesman, Improved simulation of stabilizer circuits, *Phys. Rev. A* **70**, 052328 (2004).
- [65] K. M. Audenaert and M. B. Plenio, Entanglement on mixed stabilizer states: Normal forms and reduction procedures, *New J. Phys.* **7**, 170 (2005).
- [66] D. Fattal, T. S. Cubitt, Y. Yamamoto, S. Bravyi, and I. L. Chuang, Entanglement in the stabilizer formalism, [arXiv:quant-ph/0406168](https://arxiv.org/abs/quant-ph/0406168).
- [67] M. J. Gullans and D. A. Huse, Scalable Probes of Measurement-Induced Criticality, *Phys. Rev. Lett.* **125**, 070606 (2020).
- [68] R. Vasseur, A. C. Potter, Y.-Z. You, and A. W. W. Ludwig, Entanglement transitions from holographic random tensor networks, *Phys. Rev. B* **100**, 134203 (2019).
- [69] T. Zhou and A. Nahum, Emergent statistical mechanics of entanglement in random unitary circuits, *Phys. Rev. B* **99**, 174205 (2019).
- [70] Y. Li, R. Vasseur, M. P. A. Fisher, and A. W. W. Ludwig, Statistical mechanics model for clifford random tensor networks and monitored quantum circuits, [arXiv:2110.02988](https://arxiv.org/abs/2110.02988).
- [71] T. Senthil and S. N. Majumdar, Critical Properties of Random Quantum Potts and Clock Models, *Phys. Rev. Lett.* **76**, 3001 (1996).
- [72] K. Damle and D. A. Huse, Permutation-Symmetric Multicritical Points in Random Antiferromagnetic Spin Chains, *Phys. Rev. Lett.* **89**, 277203 (2002).
- [73] M. Ippoliti, T. Rakovszky, and V. Khemani, Fractal, Logarithmic, and Volume-Law Entangled Nonthermal Steady States via Spacetime Duality, *Phys. Rev. X* **12**, 011045 (2022).
- [74] A. Nahum, J. Ruhman, and D. A. Huse, Dynamics of entanglement and transport in one-dimensional systems with quenched randomness, *Phys. Rev. B* **98**, 035118 (2018).
- [75] D. S. Fisher, Activated dynamic scaling in disordered systems, *J. Appl. Phys.* **61**, 3672 (1987).
- [76] <http://oarc.rutgers.edu>.
- [77] R. Pordes, D. Petravick, B. Kramer, D. Olson, M. Livny, A. Roy, P. Avery, K. Blackburn, T. Wenaus, F. Würthwein, I. Foster, R. Gardner, M. Wilde, A. Blatecky, J. McGee, and R. Quick, The open science grid, *J. Phys.: Conf. Ser.* **78**, 012057 (2007).
- [78] I. Sfiligoi, D. C. Bradley, B. Holzman, P. Mhashilkar, S. Padhi, and F. Würthwein, The pilot way to grid resources using glidein-WMS, in *2009 WRI World Congress on Computer Science and Information Engineering* (IEEE, New York, 2009), Vol. 2, pp. 428–432.